Available online at www.sciencedirect.com

ScienceDirect

Energy Procedia 77 (2015) 677 – 686

Energy Procedia

5th International Conference on Silicon Photovoltaics, SiliconPV 2015

Pattern of partial rear contacts for silicon solar cells

Félix Gérenton[1]*, Fabien Mandorlo[1], Jean-Baptiste Brette[2], Mustapha Lemiti[1]

[1]*Université de Lyon, Institut des Nanotechnologies de Lyon INL-UMR5270, INSA de Lyon, CNRS, 69621 Villeurbanne, France*
[2]*S'TILE, 3 rue Raoul Follereau, 86000 Poitiers, France*

Abstract

Partial rear contacts solar cells, which are passivated and locally contacted on their rear side, are widely used for their higher performances, especially in open-circuit voltage. If the distance in between two contacts has been optimized, the best geometry of a contact lattice remains unclear. So far, the most widely explored geometry is the square lattice. This work aims to explore, by the mean of numerical simulations on both PERL and PERT architectures, the consequences of different lattice geometries, and more specifically triangular and hexagonal patterns. This study was extended to the variation of a set of material and process parameters in order to observe the consequences on conversion efficiency for each contact pattern. Once the simulations performed, it has been demonstrated that even though these three geometries show the same optimal efficiency when varying the distance in between two contacts, the triangular contact pattern is clearly more robust with the variation of this distance, which makes it a good candidate for fully optimized solar cells. Moreover, the variation of material and process parameters shows the interest of the triangular contact pattern in case of degraded parameters.

Peer review by the scientific conference committee of SiliconPV 2015 under responsibility of PSE AG

Keywords: PERL, PERT, rear contacts, silicon solar cells

1. Introduction

Surface recombination is responsible for a large drop of open-circuit voltage (V_{oc}) in silicon solar cells, inducing a loss of efficiency. In order to address this problem at the rear side of a cell, one can use Partial Emitter Rear Locally diffused (PERL) or Passivated Emitter Rear Totally diffused (PERT) architectures, which consist in

* Corresponding author. Tel.: +33-472-43-74-73; fax: +33-472-43-85-31.
E-mail address: felix.gerenton@insa-lyon.fr

Peer review by the scientific conference committee of SiliconPV 2015 under responsibility of PSE AG
doi:10.1016/j.egypro.2015.07.097

depositing an insulating and poorly recombinant layer at the rear side of the absorber, then making a local ablation in order to contact the absorber with metal by point contacts regularly spread onto the surface [1]. This solution leads to a higher V_{oc}, although it also decreases the fill factor (FF) by lengthening the majority carrier path in the semiconductor. The optimization of the distance in between two localized contacts (pitch) has been widely studied [2-4], and brought to a high increase in efficiency.

These optimizations have been made assuming a square pattern for the contact lattice. However, the available ablation techniques (optical lithography [1] or ultra-violet laser [5, 6]) give the possibility of using different patterns, like the three regular ones, triangular, square and hexagonal. For a given pitch, the different lattices will change both the maximum majority carrier path (which drives the V_{oc}) and the ratio between the contacted area and the rear side surface (which drives the FF), also called metallization fraction. Therefore, the aim of this work is to compare the influence of different rear side contact patterns on the electrical performances of both PERL and PERT solar cells. After a qualitative analysis of contact patterns, complete solar cell simulations are performed for the different patterns and for different pitches. Then, the influence of different material and process parameters is studied.

2. Geometrical considerations

A scheme of the simulated device, as well as the three possible contact lattices disposed in regular patterns and the simulation domains is presented in Fig. 1. The choice of contact pattern can influence two electrical parameters: open-circuit voltage (V_{oc}) and fill factor (FF). More specifically, the V_{oc} is degraded with an increase of metallization fraction [3], called *f*. Furthermore, the FF being linked to the series resistance into the cell, and considering a constant resistivity over the substrate, one can conclude that the FF will decrease as the pitch increases. More precisely, one can find, for each contact pattern, the maximal distance p_{max} that a charge carrier can be from its closest contact on the rear contacts surface. If this distance is minimized, then the substrate resistance from this critical position to the electrode is minimized, and so the resistance for every point on the rear contacts surface is minimized, since every charge carrier will be closer to a contact than this distance. This result can be extrapolated to the charge carriers that are not onto the surface, because p_{max} will be reduced in the same way for these. Hence, the computation of *f* and p_{max} for the different geometries can enlighten the pertinence of these contact patterns.

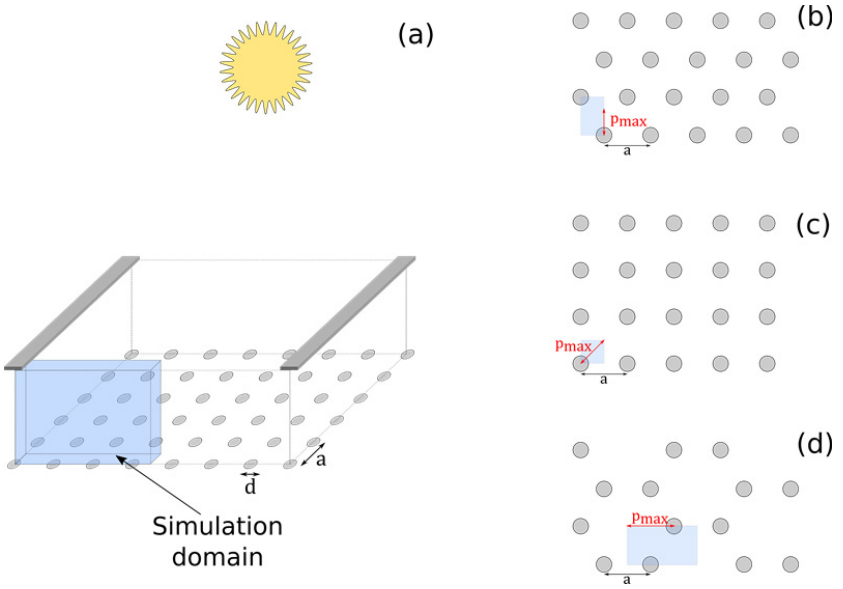

Fig. 1. (a) Sketch of the simulated device. d is the rear contact diameter and a the rear contact pitch. (b) Triangular, (c) square, (d) hexagonal rear contact patterns. Blue rectangles are the reduced simulation domain.

The unit cells of the different geometries are plotted in Fig. 1. Taking in consideration the pitch a and the contact diameter d, one can compute f and p_{max} for each contact geometry. The values of f for the triangular, square and hexagonal geometries are respectively $0.91(d/a)^2$, $0.79(d/a)^2$ and $0.60(d/a)^2$. In the same way, the values of p_{max} are respectively $0.58a$, $0.71a$ and a.

Hence, at a given pitch and contact diameter, the V_{oc} will be improved the most by the hexagonal pattern, which exhibits the smallest value of f, then by the square, and finally the triangular one. In the same way, the FF will be better using the triangular pattern, then the square, and finally the hexagonal one. The efficiency of a solar cell taking into account both FF and V_{oc}, finding the optimal contact pattern is not trivial, and can only be solved by the mean of numerical simulations.

3. Simulation setup

3.1. Simulation conditions

Numerical simulations are performed on the software Quokka [7], based on the CoBo method [8]. This simulation method presents the advantage of velocity over a FDTD simulation while obtaining similar results for standard silicon solar cells [7, 9], and allows 3D simulations, more accurate than 2D simulations to describe partial rear contact structures [10].

This work is made considering p-type, 1 Ω.cm, 180 µm thick wafers, with a front side n+ emitter and a p+ back-surface field (BSF) limited to the contacts area or not whether we consider a PERL or a PERT solar cell. The photogeneration rate is calculated considering a texturation and an anti-reflection coating on the front surface.

Simulation domains are plotted in blue in Fig. 1, and other fixed simulation parameters are specified in Table 1.

Table 1. Default simulation parameters

Geometric parameters	Cell thickness	180 µm
	Finger pitch	1 mm
	Finger width	100 µm
	Rear contact diameter	100 µm
Bulk	Substrate resistivity	1 Ω.cm
	Bulk carrier lifetime	100 µs
	Intrinsic carrier density	$9.59 \cdot 10^9$ cm^{-3}
Front side	Current recombination (non-contacted surf.)	30 fA/cm²
	Current recombination (contacted surf.)	400 fA/cm²
	Sheet resistance	30 Ω/□
	Junction depth	2 µm
	Specific contact resistivity	10 mΩ.cm
Rear side	Surface recombination velocity (non-contacted surf.)	20 cm/s
	Current recombination (contacted surf.)	400 fA/cm²
	Sheet resistance	20 Ω/□
	Junction depth	10 µm
	Specific contact resistivity	1 mΩ.cm

Fig. 2 specifies the differences between PERL and PERT structures considered in the simulations. In Quokka, emitter and BSF are described as conductive boundaries, defined by their sheet resistances, junction depths and surface recombination. Here, the electrical properties of the rear conductive boundaries are supposed identical between PERL and PERT cells, with only the shape of these conductive boundaries changing: covering the entire rear surface for PERT, and limited to the contact area for PERL cells. Moreover, the surface recombination velocity at the rear passivated interface is considered identical whether the whole surface is conductive (PERT) or only the contact area (PERL).

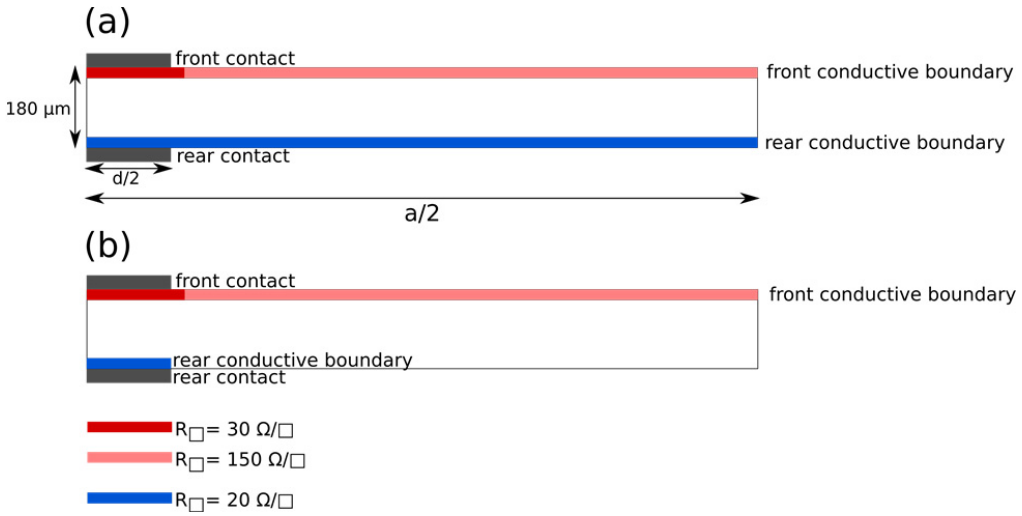

Fig. 2. Scheme of (a) PERT and (b) PERL cells representations in the simulation setup. Each color corresponds to a different conductive boundary with an indicated value of sheet resistance. a and d are respectively the rear pitch and the rear contact diameter.

In a first time, simulations are performed for the three geometries, for both PERT and PERL architectures, and for a pitch varying from 200 to 2000 µm. In a second time, we study the influence of different material parameters that can vary from the original material quality and the process: bulk lifetime, surface recombination velocity and specific back-contact resistivity.

3.2. Limitations for the hexagonal pattern

Due to software specifications, it is not possible to simulate circular contacts for the hexagonal pattern. Therefore, square shaped contacts are used. Their equivalence for our solar cell simulations is proven by simulating both contact shapes on 1 mm pitch with square contact patterns solar cells, and observing that the largest difference in the cells performances is 0.4%, for the V_{oc}. FF and efficiency stay identical for both contact shapes.

4. Simulation results

4.1. PERL

Results of simulations on PERL structures with the default parameters of Table 1 are plotted in Fig. 3. As predicted, the FF goes decreasing with the pitch, with a higher value for the triangular pattern than for the square and hexagonal ones. In the same way, the V_{oc} goes increasing, with the hexagonal pattern on top. This confirms the expectations of part 2. that at a given pitch, the FF is improved the most by the triangular pattern, and the V_{oc} by the hexagonal one.

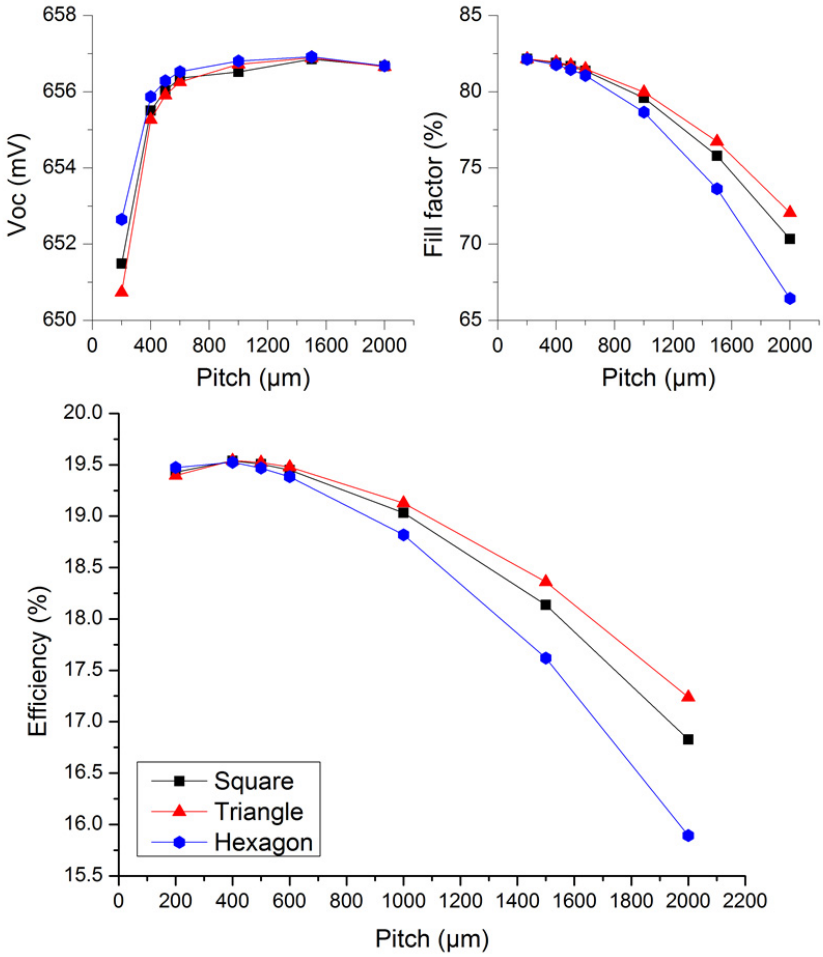

Fig. 3. (a) V_{oc}, (b) FF and (c) efficiency vs. pitch for triangular, square and hexagonal contact geometries.

Moreover, let us note that at a small pitch, the drop of FF between triangular and hexagonal pattern is very weak (0.03% of relative drop from the triangular pattern to the hexagonal one at a 200 µm pitch) while the increase of V_{oc} is more important (650.7 mV and 652.7 mV respectively, so 0.3% of relative increase). Considering this time a large pitch, the drop of FF between triangular and hexagonal pattern (7.9% of relative drop at 2000 µm pitch) is predominant in front of the increase of V_{oc} (0.003% of relative increase). These results explain the superiority of hexagonal pattern at small pitches (more gain in V_{oc} than loss in FF) and triangular pattern at large pitches (more gain in FF than loss in V_{oc}).

Furthermore, the V_{oc} increase and the FF decrease with the pitch lead to an optimum in efficiency regard to the pitch. This can be observed for every pattern in Fig. 3, and at the same pitch for approximately the same value. Thus, for this particular cell architecture, no contact pattern leads to a higher efficiency if the pitch is optimized. However, for a non-optimal pitch, either triangular or hexagonal contact pattern must be privileged.

4.2. Comparison of PERL and PERT structures

The same simulation is performed on a PERT solar cell. The results are overlapped with the previous ones on Fig. 4. As for PERL cells, the maximal conversion efficiency is found at the same pitch with roughly the same

value, the triangular pattern is to be privileged for large pitches and the hexagonal one for low pitches. However, one can note that the maximal efficiency for PERT is slightly above the one for PERL, and the efficiency is much more independent from pitch variation: from 400 to 2000 µm pitch, the efficiency for PERL drops by 2.3%, and by 0.6% for PERT (in the case of triangular pattern). This effect, already analyzed in previous works [2, 3] for the square pattern, is a consequence of a very large drop of FF with pitch for PERL cells: between 200 and 2000 µm pitch, the FF drops by 2.9% for PERT and 10.1% for PERL. Thus, the BSF on the full rear surface of PERT solar cells gives a much lower series resistance, which increases the final efficiency for large pitches. However, at the optimal pitch, the effect is moderate because of the already low series resistance, which explains the small difference of efficiency between PERL and PERT at the optimal pitch. Finally, if the maximal achievable efficiency is not really improved by PERT architecture, the pitch optimization becomes less critical.

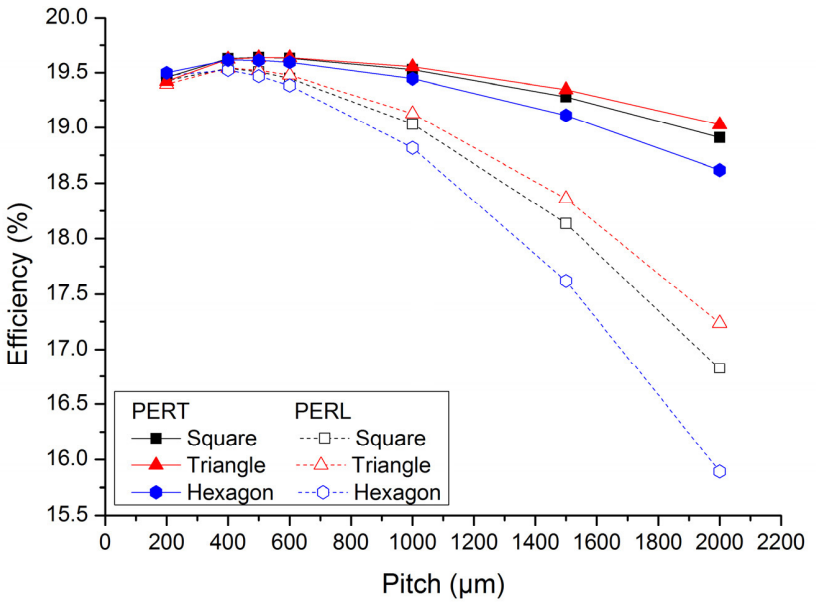

Fig. 4. Efficiency for PERL and PERT cells at different pitches and for triangular, square and hexagonal contact patterns.

4.3. Impact of material and process parameters

The pitch chosen for a design can be applied on a solar cell with a high precision, by mean of optical lithography or laser ablation. Thus, the efficiency being stable around the optimal pitch as in Fig. 3, the choice of a specific contact pattern is not critical if we consider the material and process parameters to be perfectly known. However, if these parameters are not perfectly mastered during cell fabrication, the optimal pitch can be miscalculated, leading to a drop in efficiency. If this drop cannot be avoided, it can be minimized by a good choice of contact pattern. Indeed, as seen in Fig. 3, out of the optimal pitch, the best efficiency is not achieved by all the contact patterns at the same time. In order to find the most adapted contact pattern to address this problem, three parameters have been chosen for study: surface recombination velocity (SRV) S_{eff} at the rear side, bulk carrier lifetime τ_{bulk} and specific contact resistivity ρ_c for the rear contacts. These parameters can all vary from one cell to another, according to the process conditions or the initial material quality.

Fig. 5 shows the simulated efficiencies of PERL solar cells with S_{eff} set at 10, 100 and 1000 cm/s (maintaining doping level and junction depth constant in the BSF). The maximal efficiency decreases with S_{eff} as expected, and the optimal pitch is shifted towards low values, for all contact patterns. This can be understood by the fact that

surface recombination becoming higher and higher, the difference with the recombination at the rear contacts becomes smaller, and so the metallization fraction becomes less critical.

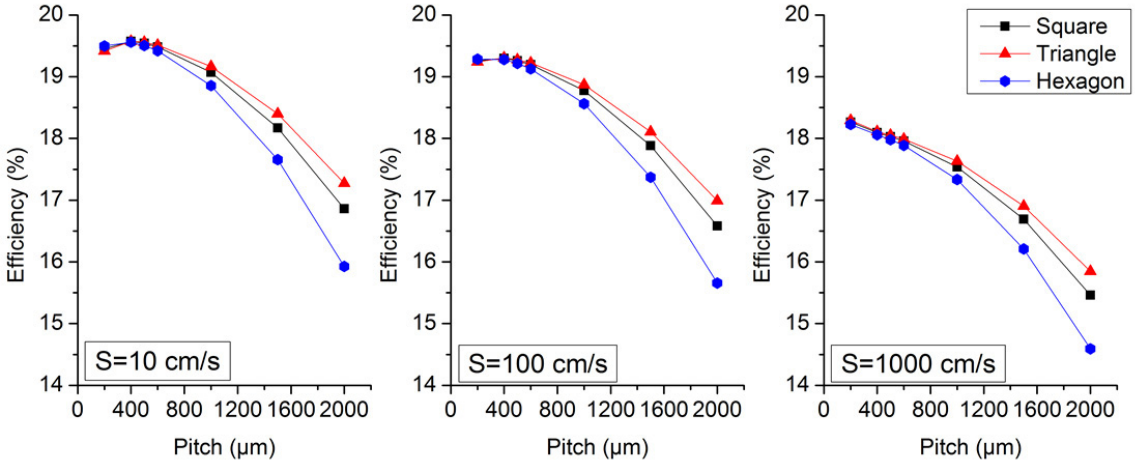

Fig. 5. Efficiency for PERL cells with different pitches, values of S_{eff} and for triangular, square and hexagonal patterns.

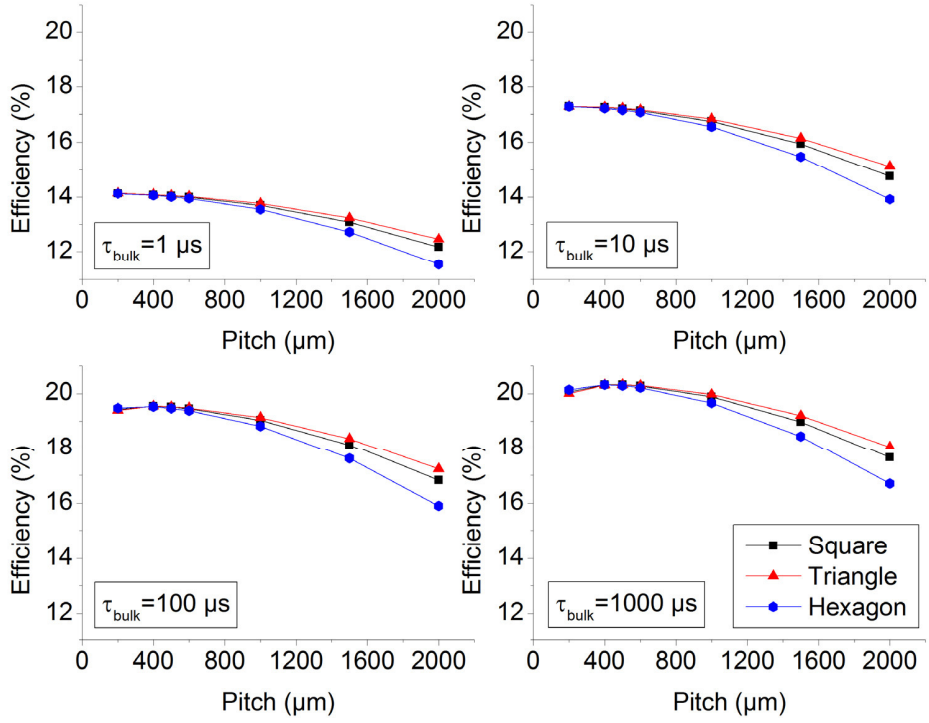

Fig. 6. Efficiency for PERL cells with different pitches, values of τ_{bulk} and for triangular, square and hexagonal patterns.

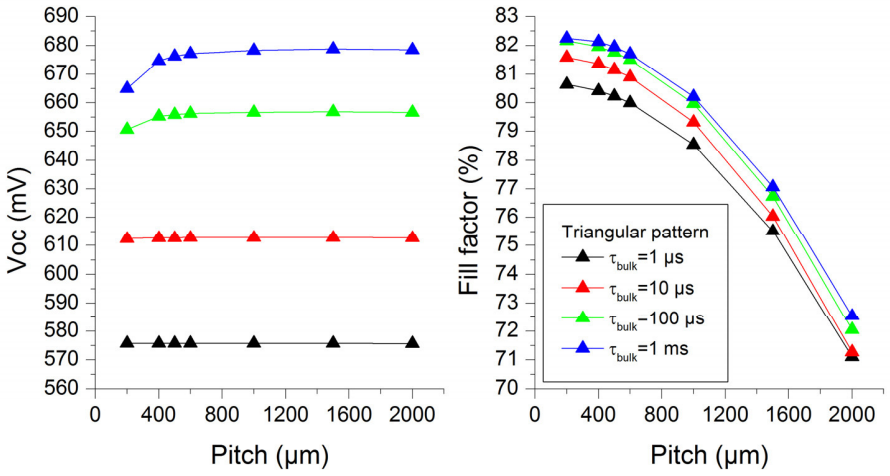

Fig. 7. V_{oc} and FF of PERL cells with triangular contact patterns, for different pitches and τ_{bulk}.

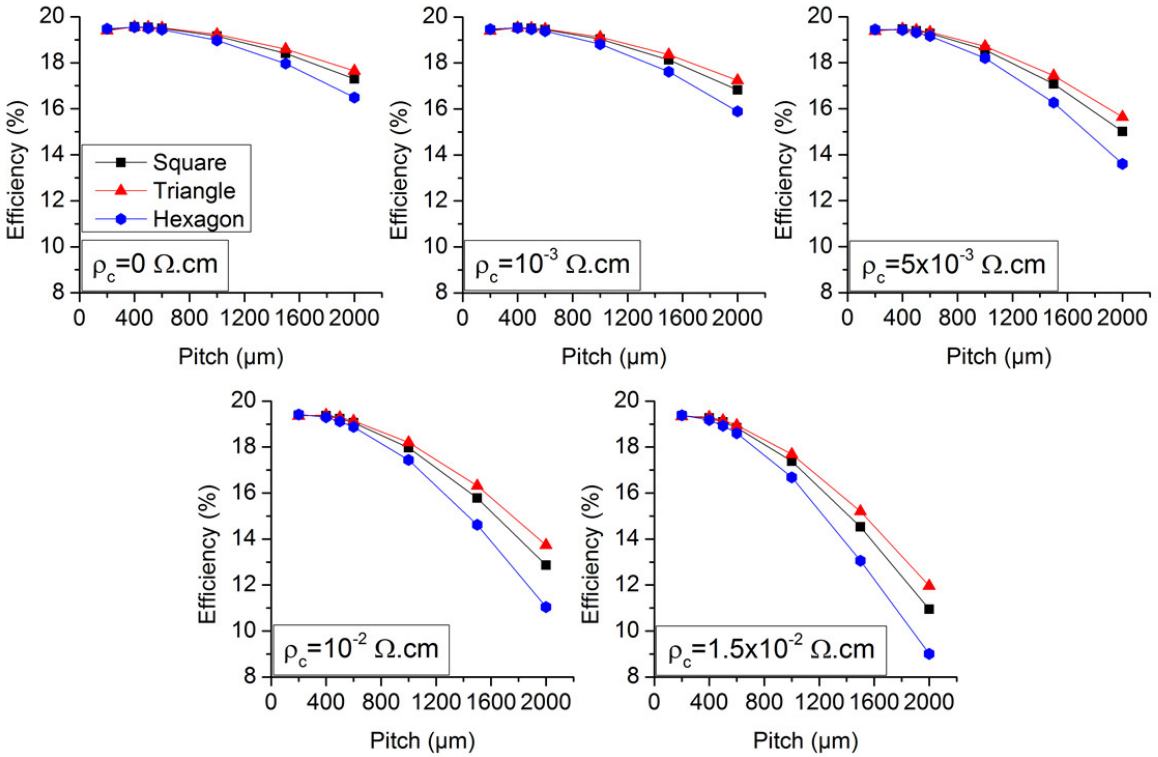

Fig. 8. Efficiency of PERL cells with different pitches, values of ρ_c and for triangular, square and hexagonal patterns.

In Fig. 6, one can observe the effect of τ_{bulk} (from 1 µs to 1 ms) on the conversion efficiency for PERL cells: here again, both the maximal efficiency and the optimal pitch decrease with the decrease of τ_{bulk}. To explain this shift, let us compare in Fig. 7 the drop of V_{oc} between the optimal pitch and a lower pitch (400 and 200 µm respectively), for a high and a low τ_{bulk} (1 µs and 1 ms): the drop of Voc is 9.7 mV for τ_{bulk}=1 ms and less than 0.1 mV for τ_{bulk}=1 µs. This can be explained considering that at a low τ_{bulk}, the surface recombination will become negligible in front of the volume recombination, and so the pitch would not affect the V_{oc} significantly. The consequence of this difference of V_{oc} drop finally proves the optimal pitch shift: at low τ_{bulk}, the V_{oc} being almost constant with the pitch, the efficiency will follow the FF curve, which decreases with the pitch.

Finally, the variation of ρ_c from 0 to 15 mΩ.cm is shown in Fig. 8 (again, no change in the BSF parameters): here, the drop of maximal efficiency with the increase of ρ_c is not important, but the shift of the optimal pitch to low values is still present. The explanation for this shift is, as shown in Fig. 9, that the FF strongly decreases with ρ_c while the V_{oc} remains unchanged. Moreover, the drop of FF increases with the pitch. Consequently, efficiencies at large pitches will be strongly affected by an increase of ρ_c, and will remain constant at low pitches. Thus, the maximal efficiency will occur at a lower pitch. This study is in agreement with the study led in [3] in the case of square contact patterns.

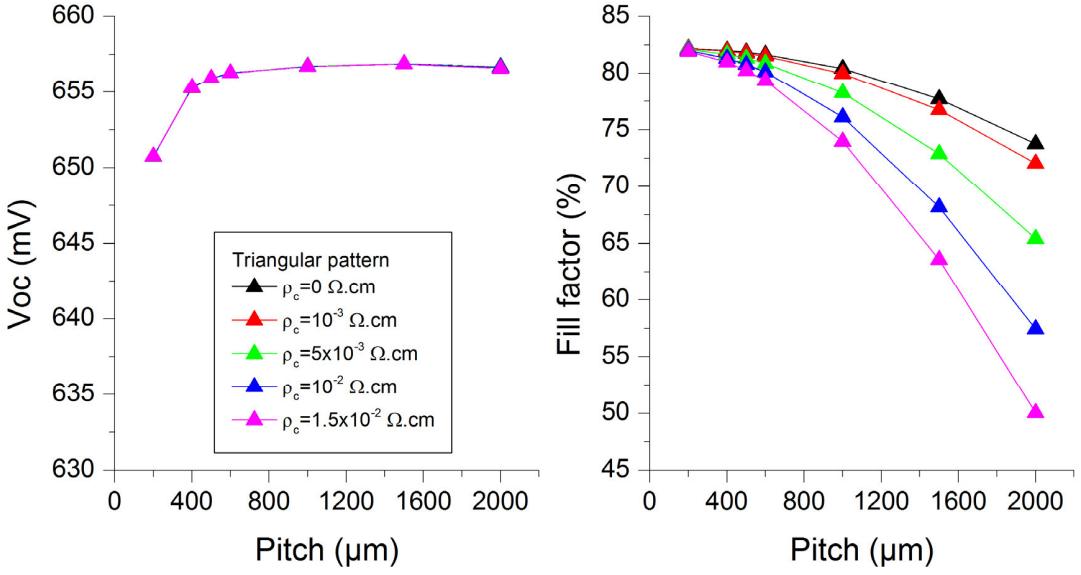

Fig. 9. V_{oc} and FF of PERL cells with triangular contact patterns, for different pitches and ρ_c.

Among the three parameters studied, different mechanisms have led to one common result: the shift of the optimal pitch to lower values with the degradation of parameters. If generalizing this statement to a large number of material and process parameters is beyond the scope of this work, let us note that the parameters studied here have a big influence on the final cell performances, and are not easily controllable. Thus, their effect can be taken into account for a solar cell design by using the contact pattern leading to the best efficiency with degraded parameters at the optimal pitch, which is, as it can be seen in Fig. 5, 6 and 8, the triangular contact pattern. This way, a solar cell designed taking into account non-degraded parameters will be less affected (in terms of conversion efficiency) in case of degraded parameters using the triangular pattern.

5. Conclusion

In this study, we have shown the interest of using different rear contact patterns (triangular, square and hexagonal geometries) for optimizing the efficiency of PERL or PERT silicon solar cells. It has been demonstrated that, for an optimized PERL or PERT cell without degradation in material or process parameters (surface recombination velocity, bulk carrier lifetime and specific contact resistivity in this study), the choice of contact pattern does not significantly influence the cell efficiency. However, the choice of a triangular contact pattern can prevent from some of the losses due to an eventual degradation of the parameters quoted above. Moreover, the mechanisms explaining the differences caused by the different contact patterns have been enlightened; especially the superiority of the hexagonal pattern at low pitches and of the triangular one at high pitches.

Acknowledgements

Dr. Andreas Fell from Australian National University is gratefully acknowledged for his help with the simulation software.

References

[1] Blakers A, Wang A, Milne AM, Zhao J, Green M. 22.8% efficient silicon solar cell. Appl Phys Lett 1989;55(13):1363-1365.
[2] Cuevas A. Electrons and holes in solar cells with partial rear contacts. Prog Photovolt: Res Appl 2013;20:31-43.
[3] Zanuccoli M, De Rose R, Magnone P, Sangiorgi E, Fiegna C. Performance analysis of rear point contact solar cells by three-dimensional numerical simulation. IEEE Trans Electron Devices 2012;59(5):1311–1319.
[4] De Rose R, Van Wichelen K, Tous L, Das J, Dross F, Fiegna C, Lanuzza M, Sangiorgi E, Uruena De Castro A and Zanuccoli M. Optimization of rear point contact geometry by means of 3-d numerical simulation. Energy Procedia 2012;27:197–202.
[5] Glunz SW, Preu R, Schaefer S, Schneiderlochner E, Pfleging W, Ludemann R, Willeke G. New simplified methods for patterning the rear contact of RP-PERC high-efficiency solar cells. Conference Record of the Twenty-Eighth IEEE Photovoltaic Specialists Conference, Anchorage, Alaska, USA; 2000. p. 168–171.
[6] Schneiderlochner E, Preu E, Ludemann R, Glunz SW. Laser fired rear contacts for crystalline silicon solar cells. Prog Photovolt: Res Appl 2002;10(1):29–34.
[7] Fell A. A free and fast three-dimensional/two-dimensional solar cell simulator featuring conductive boundary and quasi-neutrality approximations. IEEE Trans Electron Devices;60(2):733–738.
[8] Brendel R. Modeling solar cells with the dopant-diffused layers treated as conductive boundaries. Prog Photovolt: Res Appl 2012;20(1): 31–43.
[9] Cuevas A, Yan D, Haase F, Petermann JH, Brendel R. A comparison of models to optimize partial rear contact solar cells. Energy Procedia 2013;38:13–21.
[10] López-González JM, Martín I, Ortega P, Orpella A, Alcubilla R. Numerical simulations of rear point-contacted solar cells on 2.2 ohm.cm p-type c-si substrates. Prog Photovolt: Res Appl 2015;23:69-77.